pISSN 2384-1095
eISSN 2384-1109

iMRI 2020;24:67-75

https://doi.org/10.13104/imri.2020.24.2.67

iMRI
Investigative Magnetic Resonance Imaging

RF Heating of Implants in MRI: Electromagnetic Analysis and Solutions

Youngdae Cho, Hyoungsuk Yoo

Department of Biomedical Engineering, Hanyang University, Seoul, Korea

When a patient takes an MRI scan, the patient has a risk of unexpected injuries due to the intensive electromagnetic (EM) field. Among the injuries, the tissue heating by the time-varying EM field is one of the main issues. Since an implanted artificial structure with a conductive material aggravates the heating effect, lots of studies have been conducted to investigate the effect around the implants. In this review article, a mechanism of RF heating around the implants and related studies are comprehensively investigated.

Keywords: Radio Frequency; Heating; Implants; RF coils

Review Article

Received: March 1, 2020
Revised: March 29, 2020
Accepted: April 6, 2020

Correspondence to:
Hyoungsuk Yoo, Ph.D.
Department of Biomedical Engineering, Hanyang University, 222, Wangsimni-ro, Seongdong-gu, Seoul 04763, Korea.
Tel. +82-2-2220-2306
Fax. +82-2-2296-5943
E-mail: hsyoo@hanyang.ac.kr

INTRODUCTION

Recently, a magnetic resonance imaging (MRI) has become an indispensable medical imaging device. Unlike a computed tomography (CT) system, the MRI has an advantage of acquiring an anatomical image using a magnetic field without tissue ionizing. However, as a patient taking MRI scan is exposed to a much stronger electromagnetic field than in everyday life, there is a risk of unwanted electromagnetic reactions in the human body. Except for an interaction with a static magnetic field (B_0) generated by a main magnet, RF heating, increase of the tissue temperature due to a RF magnetic field (B_1) transmitted by RF coil, is the major concern. In this review article, some studies related to the RF heating in the MRI are extensively analyzed. Especially, researches regarding the artificial products such as implantable medical devices (IMDs) and tattoos which aggravate the RF heating are mainly discussed in the article.

Safety Guidelines and Concerns During MR Examination

To obtain an anatomical image through a signal contrast depending on the tissues, the patient is exposed to strong magnetic fields such as static field B_0 and time-varying field B_1 during the MRI scan. One of the main risks by the B_0 field is a magnetic pulling. The ferromagnetic materials such as steel and nickel are highly attracted toward the MR bore when placed in the region of the strong magnetic field with strong magnetic field gradients (1-4). Therefore, carrying the products which could be highly affected by the magnetic field are strictly prohibited.

When the B_1 field is applied to a patient, some part of RF energy is deposited in the human body and triggers the temperature rise when a quantity of the absorbed

energy exceeds the limit which can be controlled by the thermoregulation (4-7). To assess the thermal effect due to the exposure of electromagnetic waves, a normalized rate of energy absorbed in the tissues called SAR (specific absorption rate) is evaluated. SAR within the tissue located at point $r = (x, y, z)$ can be calculated by Eq. [1] as

$$SAR = \frac{\sigma(r)|E(r)|^2}{2\rho} \quad [1],$$

where σ is the electrical conductivity (S/m), E is the electric field (V/m), and ρ is the mass density of the tissue (kg/m^3). Since SAR is proportional to an intensity of the RF source, the total power of the transmit electromagnetic field should be scaled to keep the SAR below the limit regulated by the international electrotechnical commission (IEC) as given in Table 1 (8, 9).

Even though the limit varies depending on the operating mode, the values based on the normal mode is mainly considered to be safe for most of the patients including those with lower thermoregulatory capacity. Local SAR of the partial body listed on the table is averaged over the mass of 10 g.

MRI-Induced RF Heating at Implantable Medical Devices

An implantable medical devices (IMD) is inserted inside a human body semi-permanently. The IMD can be classified into passive type and active type. The passive implants compensate for the insufficient physical function of an organ inside of the human body e.g., hip implant. While, the active implants restore some functions of the body parts or relieve a pain through electrical stimulation. Unlike some on-body worn decorative accessories, it is practically impossible to exclude the IMDs from the patients during the MRI scan. Therefore, a metallic part of the devices should be made with a paramagnetic or diamagnetic metal having low magnetic susceptibility to prevent the magnetic pulling and an image distortion due to the implantable device (10, 11).

Table 1. IEC SAR standards for MR scanning

Operating mode		Normal	1st-level controlled	2nd-level controlled
Whole Body SAR		2	4	>4
Head SAR		3.2	3.2	>3.2
Local SAR	Head	10	20	>20
	Trunk	10	20	>20
	Extremities	20	40	>40

IEC = international electrotechnical commission; SAR = specific absorption rate

According to the Maxwell-Faraday equation (Eq. [2]) shown as follows

$$\oint_C E \cdot dl = -\iint_S \frac{\partial B}{\partial t} \cdot dS, \quad [2]$$

voltage around the stationary closed loop c is equal to the rate of change in the magnetic flux density B over time integrated over the surface enclosed by the loop S. During the MRI scan, a RF pulse called B_1 is applied to a human body to induce spin excitations of target nuclei. The time-varying magnetic pulse generates eddy currents at the metal plate of the implants as predicted by the Eq. [2]. The eddy currents can heat up the metal plate by joule heating or the tissues by flowing itself to the tissues in contact with the implants (12-17). Especially, a structure of a conductive wire such as a lead of artificial cardiac pacemaker (PM) and deep brain stimulator (DBS) acts like an antenna which significantly absorbs external RF energy to increase heating (18-30). The currents generated at the whole wire flow along the path and are accumulated at the tip of the lead wire. Since the excessive amounts of energy by the unwanted currents are transferred into the contiguous tissues, the risk of RF heating increases significantly that electrode dropout and a permanent tissue damage can occur.

For the reason mentioned above, the implanted medical wires are considered as the major risk of RF heating in the MRI and most of the studies of MRI-induced RF heating are extensively carried out on this issue. To analyze the effect and develop a mitigation method of RF heating around the lead, a numerical simulation based on some electromagnetic solvers is an alternative and widely used technique to cover the infeasibility of clinical trials due to the safety issues (30-34). In the following chapter, procedures of the EM and thermal simulations are briefly explained. In addition, studies to reduce the RF heating and validate the simulated results with the measurements are also introduced.

1. Numerical Analysis of RF Heating

For the numerical analysis to understand the electromagnetic phenomenon inside of the human body, commercial simulation softwares were developed.

Depending on the numerical method to solve problems, for example, COMSOL and ANSYS HFSS using finite element method (FEM), Sim4life and XFdtd using finite-difference time-domain method (FDTD), and CST using finite integration method (FIM) are widely used. To analyze a target object, the whole object is decomposed into smaller parts termed as finite elements. Depending on the shape of the element, a voxel and a mesh is usually used for the cubic and triangular shapes, respectively. By assembling the solutions of the simplified differential equations based on the Maxwell equations from each element region, the electromagnetic effect in whole object can be approximately predicted. Based on the data obtained from EM simulations, the amount of temperature rise by RF exposure is calculated by thermal simulation based on the bio-heat equation (35-37). The formula (Eq. [3]) is expressed as

$$\rho c \frac{dT}{dt} = \nabla \cdot (k \nabla T) + \rho Q + \rho S - \rho_b c_b \rho w (T - T_b) \quad [3]$$

where, Q is the metabolic heat generation rate, w is the perfusion rate, c is the heat capacity, S is SAR, T is the current temperature of the tissue, and k is the thermal conductivity. The symbols with subscript b represents the coefficients of the blood. The term '$\rho_b c_b \rho w$' is referred as the heat-transfer rate. Except the value of T, all parameters in the formula are tissue-specific quantities which are assigned automatically when the realistic human phantom is provided.

2. Modeling for Simulation

Regardless of the type of the simulation, making a realistic 3-D computer aided design (CAD) of the target object is the first step to minimize an error during the approximation. The studies in the early stage used a simple-shaped single-layered human phantom with uniform material properties due to the difficulty in realistic human body modeling. Fortunately, current softwares based on FDTD provide their own human models like Virtual Population (ViP) models of IT'IS Foundation, Switzerland and CST Voxel Family by Dassault Systems, France. Thanks to the models composed of various tissues having different electric properties, reliability of the numerical study related to RF heating has been increased (38).

As we mentioned above, a designed model in the simulation domain are divided into the several finite elements for a calculation based on the electromagnetic equations. An accuracy of the simulated result is directly affected by setting the size of an element called 'grid'. Although a tightly spaced grid in the target objects is essential to get the result with higher reliability, the compactness of each grid below a certain volume exceeding the computing capacity of the users cannot be assigned. During the numerical simulations, the components of computing hardware mainly influence the calculation efficiency. Features of CPU such as a clock rate and the number of cores are significantly related to a computation time. The size of RAM determines the speed of the simulation processed as a single task. Since the required space and the required time for the simulation are proportional to the number of the total elements, it is very important to set up a balance in the trade-off of gridding which satisfies both short computation time and small approximation error.

Figure 1 shows depicted models of a human body and an implanted lead wire in the FDTD-based simulation depending on the different gridding size. Compared to the human model in Figure 1a, the lead model in Figure 1b has smaller and complicated structure with the dimensions in millimeters that accuracy of the results varies very sensitively by the size of grid. Since the lead wire is the major component among other IMDs to cause RF heating in MRI, setting its grid with extremely fine size is essential in the simulation for higher accuracy, even if a massive amount of memory and storage capacity is required.

Due to the limited computing resources, most of the RF heating studies in the early stages has used a simplified form of lead composed of a single conductive wire and an insulation layer with the same diameter as the actual cable (28, 30, 39-44). However, in the simplified lead model, an error of electric field which is the main source to evoke the RF heating has inevitably occurred. To alleviate the error, Feng et al. (45) developed a numerical technique to evaluate the electric fields at the lead. Using the reciprocity theorem and the Huygens principle, the electric field induced at the electrode tip is calculated with high accuracy even with the simplified lead model. In addition, Park et al. (46) introduced the transfer function to calculate the RF heating of the lead in which the magnitude and the phase of a transfer function, as well as the incident electric field along the length of the lead can be used to calculate the RF heating at the electrode.

3. Measurement Setup for Validation

Experiments are implemented to validate the simulated

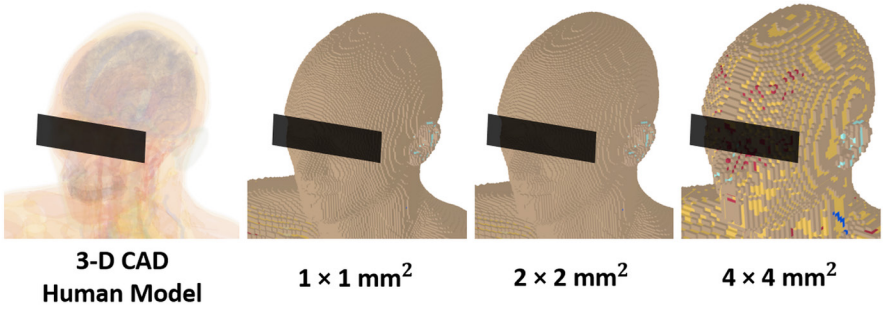

a

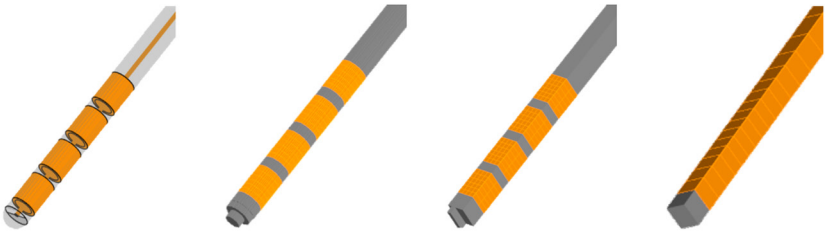

b

Fig. 1. Depicted 3-D models in simulation depending on the size of single grid. (a) A heterogeneous human model gridded with 1 mm, 2 mm, 4 mm resolution, respectively. (b) A DBS lead model (lead model 3389 : Medtronic Inc. Minneapolis, MN, USA) gridded by 0.05 mm, 0.5 mm, 2 mm resolution, respectively.

results and improve our understanding of RF heating mechanism around the implants. Considering the safety of the patients with IMDs, most of the experiments are performed in the artificial model called ASTM phantom. ASTM phantom is designed to follow American Society for Testing and Materials (ASTM) F-2182-02 (47) or F-2182-09 (48) standard for evaluation of induced heating around passive IMD exposed to MRI. To ignore the influence of the static magnetic field B_0, some studies used Medical Implant Test System (MITS) working like whole-body RF coil as the RF source (49, 50). However, it is noteworthy that a continuous wave (CW) from MITS as the transmitted signal aggravates the RF heating effects compared to the clinical coil generating the signal with the pulses for the same input power and exposure duration. Under the RF source mentioned above, B_1^+ field, incident electric field, SAR, temperature can be measured by MRI-compatible assessment system such as EASY6/MRI and DASY6 (SPEAG, Switzerland) which uses the probes with non-magnetic and shielded structure connected with optical fiber.

4. Methods to Reduce RF Heating of Implanted Lead

In response to the increasing number of the patients with the leads, various mitigating techniques have been proposed to reduce the RF heating near the IMD. An intuitive way to remove the RF heating is the EM shielding by placing the conductive plate outside the region where the IMDs are inserted (51-55). When the electromagnetic wave travels through the shield composed of metal or electro-conductive plastic, most of the energy of the wave is absorbed at the surface of the layer; the amount of the absorbed energy at the biological tissues causing heating significantly decreases. However, in the light of the RF signals for an image acquisition, the RF pulse to excite the proton for imaging also absorbed by the shield, which shows an image with poor resolution at the shielded area. Furthermore, a high dielectric material (HDB) pad was used to reduce the RF-induced heating around the lead. The HDM can maintain the strength of the applied B_1 field even with the significantly low required power for imaging (56-59). However, the design of HDM are patient specific, and the manufacturing of HDM pad with dielectric constant up to 500 is challenging.

Rather than adding some external structures, methods to modify the structure of the lead itself are introduced to alleviate the RF heating (60-65). Bottomley et al. (62) shows that a helical design in the wire can reduce the heating at the tip of the lead. Also, Das et al. (63, 64) show that insertion of pins along the lead reduces the amount of the induced current flowed at the tip by changing the impedance distribution. However, the ways to modify the lead are also impractical to be used in clinic instantly

because the complex lead design also increase the difficulty of mass production. Instead, some studies try to reduce the RF heating by changing the lead path inserted in the human body. For example, Shrivastava et al. (66) and Golestanirad et al. (67) show that forming extra-cranial loops with the conventional lead can alleviate the RF heating around the electrode of DBS.

Based on the electromagnetic theory, the intensity of electric field, especially tangential electrical field which lies on the surface of the conductor, mainly affects the RF heating around the electrode. Figure 2 shows the simulated SAR distribution around DBS lead depending on the applied EM field distribution. For the RF source, multi-channel RF coil consisting of eight-microstrip transmission line (MTL) resonators working at 7 T were used, and whole input power of the coil is normalized to keep the mean of the B_1^+ on the axial slice same with 2 μT. According to the results, peak SAR was found near the DBS electrode. In addition, we found that the inhomogeneity of the RF magnetic field deteriorated locally around the electrode aggravating the RF heating. Similar to this study, some studies tried to reduce the RF heating by modifying the time-varying EM field distributions in the human body (44, 68-74). To minimize the incident electric field around the implant, proper amplitude and phase of the RF coil, which is essential to transmit a uniform magnetic field in the body, are calculated by the numerical method (75). Recently, an ultra-high field MRI over 7 T is introduced, and usually adopts the shimming technique to supplement the transmit efficiency degraded by field inhomogeneity. Therefore, the excitation control of the RF coil to achieve both acquisition of anatomical image with high resolution and alleviation of RF heating around IMD will be vigorously studied.

RF Heating around Tattoos

Except the metallic IMD, a tattoo drawn on the body permanently can be a potential risk of RF heating. During the MRI scan, some cases that patients experienced pains like burning around the tattoos are infrequently reported (76-80). Even though the reason of the cutaneous inflammation is not revealed, most accepted theory is that tattoo is working as an electrical path. Tattoo ink contains the ferromagnetic component like iron oxide for color development (81, 82). In the dyed skin tissues with the conductive tattoo ink, electric currents are induced by the external time-varying EM field. Depending on the length and shape of tattoo, tattoo can work as an antenna which absorbs high energy and causes excessive skin heating. Especially, a tattoo with loop or shape edges increases the risk of the RF heating (83).

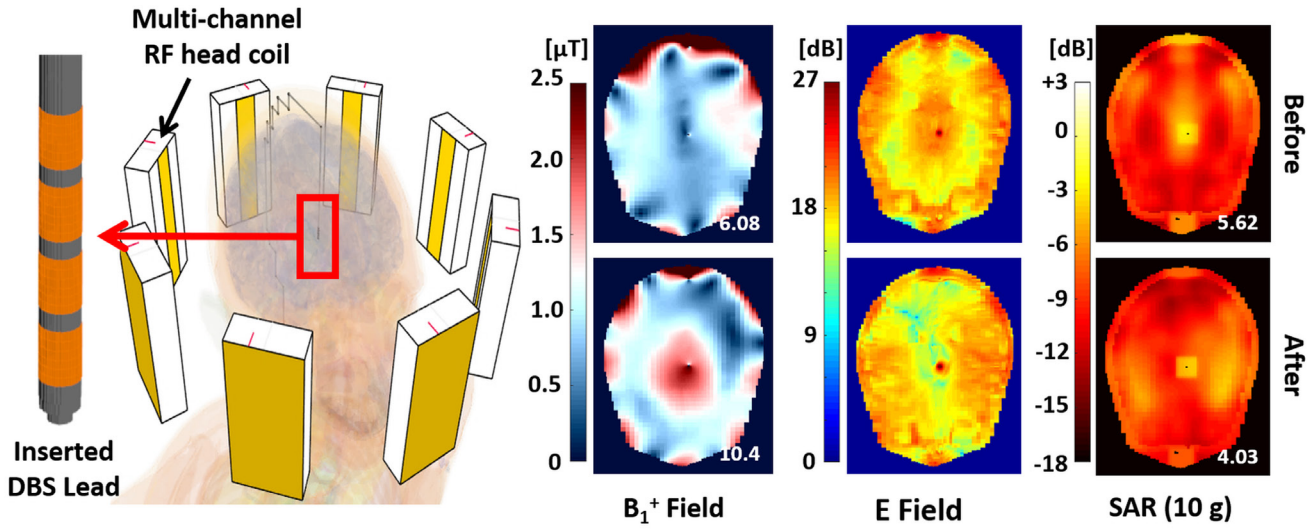

Fig. 2. A numerical study to modify the applied electromagnetic field to reduce RF heating near DBS lead. Axial slices of electromagnetic field and SAR before and after modification of the amplitude and phase of each channel of RF coil are demonstrated at the right side of the image. The slice is placed where the electrode is located. The multi-channel RF coil is set to work at 7 T with the same input power scaled to the mean of the B_1^+ on the axial slice of 2 μT. The total of the applied B_1^+ values and peak SAR of the gridded cells inside the human head is shown at the lower right corner of each plot, respectively.

For cosmetic and decorative purposes, any size and shape of the tattoos can be painted anywhere of the human body. In addition, the components and concentration of the tattoo ink are varied depending on the color and different manufacturers. To analyze the MRI-induced RF heating around the tattoos, therefore, parametric analysis including the ink, shape, size, color, and area to be drawn of the tattoo should be implemented through numerical simulations.

DISCUSSION

In this article, the safety risks by the magnetic field of MRI and the methods to analyze it are comprehensively explained. Especially, as the number of patients with the IMD have been increased, studies related to the implants with lead wire are intensively analyzed. Although most of the studies are performed by using the numerical simulations, lots of numerical techniques and measurement methods are introduced to improve the reliability of the results. The calculated results are considerably dependent on the voxel size (84), indicating that assignment of proper grid size is the key factor for the numerical simulation. Instead of the simulation, the temperature can be measured wirelessly by MR thermometry. However, RF field and flip angle, which varies depending on the temperature, need to be corrected (85). Recently, 7 T ultra-high field MRI system gets FDA approval to use for clinical trials. Since MRI with stronger magnetic field aggravates RF heating around the implants, the study to analyze and solve the RF heating of the implants exposed to 7 T MRI will be promising.

Acknowledgments

This research was supported by the Basic Science Research Program through the National Research Foundation of Korea funded by the Ministry of Science and ICT under Grant 2019R1A2C2004774.

REFERENCES

1. Gangarosa RE, Minnis JE, Nobbe J, Praschan D, Genberg RW. Operational safety issues in MRI. Magn Reson Imaging 1987;5:287-292
2. Shellock FG, Kanal E. Policies, guidelines, and recommendations for MR imaging safety and patient management. SMRI Safety Committee. J Magn Reson Imaging 1991;1:97-101
3. Shellock FG, Crues JV. MR procedures: biologic effects, safety, and patient care. Radiology 2004;232:635-652
4. Panych LP, Madore B. The physics of MRI safety. J Magn Reson Imaging 2018;47:28-43
5. Bottomley PA, Andrew ER. RF magnetic field penetration, phase shift and power dissipation in biological tissue: implications for NMR imaging. Phys Med Biol 1978;23:630-643
6. Schaefer DJ. Safety aspects of radiofrequency power deposition in magnetic resonance. Magn Reson Imaging Clin N Am 1998;6:775-789
7. Formica D, Silvestri S. Biological effects of exposure to magnetic resonance imaging: an overview. Biomed Eng Online 2004;3:11
8. IEC 60601-2-33, Medical electrical equipment - Part 2-33: Particular requirements for the safety of magnetic resonance equipment for medical diagnosis. Geneva Switzerland: IEC, 2002
9. C95.1-2005 - IEEE standard for safety levels with respect to human exposure to radio frequency electromagnetic fields, 3 kHz to 300 GHz. IEEE Std C95.1-1991
10. Schenck JF. Safety of strong, static magnetic fields. J Magn Reson Imaging 2000;12:2-19
11. Luechinger R, Duru F, Scheidegger MB, Boesiger P, Candinas R. Force and torque effects of a 1.5-Tesla MRI scanner on cardiac pacemakers and ICDs. Pacing Clin Electrophysiol 2001;24:199-205
12. Davis PL, Crooks L, Arakawa M, McRee R, Kaufman L, Margulis AR. Potential hazards in NMR imaging: heating effects of changing magnetic fields and RF fields on small metallic implants. AJR Am J Roentgenol 1981;137:857-860
13. Hartnell GG, Spence L, Hughes LA, Cohen MC, Saouaf R, Buff B. Safety of MR imaging in patients who have retained metallic materials after cardiac surgery. AJR Am J Roentgenol 1997;168:1157-1159
14. Condon B, Hadley DM. Potential MR hazard to patients with metallic heart valves: the Lenz effect. J Magn Reson Imaging 2000;12:171-176
15. Smith CD, Nyenhuis JA, Kildishev AV. Health effects of induced electrical currents: implications for implants. In Shellock FG, ed. Magnetic resonance: health effects and safety. Boca Raton, FL: CRC Press, 2001:393-413
16. Ruggera PS, Witters DM, von Maltzahn G, Bassen HI. In vitro assessment of tissue heating near metallic medical implants by exposure to pulsed radio frequency diathermy. Phys Med Biol 2003;48:2919-2928
17. Nyenhuis JA, Park SM, Kamondetdacha R, Amjad A, Shellock FS, Rezai AR. MRI and implanted medical devices: basic interactions with an emphasis on heating. IEEE T

Device Mat Re 2005;5:467-480
18. Teissl C, Kremser C, Hochmair ES, Hochmair-Desoyer IJ. Magnetic resonance imaging and cochlear implants: compatibility and safety aspects. J Magn Reson Imaging 1999;9:26-38
19. Yeung CJ, Atalar E. RF transmit power limit for the barewire loopless catheter antenna. J Magn Reson Imaging 2000;12:86-91
20. Yeung CJ, Susil RC, Atalar E. RF heating due to conductive wires during MRI depends on the phase distribution of the transmit field. Magn Reson Med 2002;48:1096-1098
21. Yeung CJ, Susil RC, Atalar E. RF safety of wires in interventional MRI: using a safety index. Magn Reson Med 2002;47:187-193
22. Nitz WR, Oppelt A, Renz W, Manke C, Lenhart M, Link J. On the heating of linear conductive structures as guide wires and catheters in interventional MRI. J Magn Reson Imaging 2001;13:105-114
23. Smith CD, Kildishev AV, Nyenhuis JA, Foster KS, Bourland JD. Interactions of MRI magnetic fields with elongated medical implants. J Appl Phys 2000;87:6188-6190
24. Achenbach S, Moshage W, Diem B, Bieberle T, Schibgilla V, Bachmann K. Effects of magnetic resonance imaging on cardiac pacemakers and electrodes. Am Heart J 1997;134:467-473
25. Sommer T, Vahlhaus C, Lauck G, et al. MR imaging and cardiac pacemakers: in-vitro evaluation and in-vivo studies in 51 patients at 0.5 T. Radiology 2000;215:869-879
26. Martin ET, Coman JA, Shellock FG, Pulling CC, Fair R, Jenkins K. Magnetic resonance imaging and cardiac pacemaker safety at 1.5-Tesla. J Am Coll Cardiol 2004;43:1315-1324
27. Angelone LM, Potthast A, Segonne F, Iwaki S, Belliveau JW, Bonmassar G. Metallic electrodes and leads in simultaneous EEG-MRI: specific absorption rate (SAR) simulation studies. Bioelectromagnetics 2004;25:285-295
28. Finelli DA, Rezai AR, Ruggieri PM, et al. MR imaging-related heating of deep brain stimulation electrodes: in vitro study. AJNR Am J Neuroradiol 2002;23:1795-1802
29. Park SM, Kamondetdacha R, Amjad A, Nyenhuis JA. MRI safety: RF-induced heating near straight wires. IEEE T Magn 2005;41:4197-4199
30. Golombeck MA, Thiele J, Dossel O. Magnetic resonance imaging with implanted neurostimulators: numerical calculation of the induced heating. Biomed Tech (Berl) 2002;47 Suppl 1 Pt 2:660-663
31. Nguyen UD, Brown JS, Chang IA, Krycia J, Mirotznik MS. Numerical evaluation of heating of the human head due to magnetic resonance imaging. IEEE Trans Biomed Eng 2004;51:1301-1309
32. Collins CM, Liu W, Wang J, et al. Temperature and SAR calculations for a human head within volume and surface coils at 64 and 300 MHz. J Magn Reson Imaging 2004;19:650-656
33. Collins CM. Numerical field calculations considering the human subject for engineering and safety assurance in MRI. NMR Biomed 2009;22:919-926
34. Hand JW. Modelling the interaction of electromagnetic fields (10 MHz-10 GHz) with the human body: methods and applications. Phys Med Biol 2008;53:R243-286
35. Guy AW, Lehmann JF, Stonebridge JB. Therapeutic applications of electromagnetic power. P IEEE 1974;62:55-75
36. Wang J, Fujiwara O. FDTD computation of temperature rise in the human head for portable telephones. IEEE Trans Microw Theory Tech 1999;47:1528-1534
37. van Lier AL, Kotte AN, Raaymakers BW, Lagendijk JJ, van den Berg CA. Radiofrequency heating induced by 7T head MRI: thermal assessment using discrete vasculature or Pennes' bioheat equation. J Magn Reson Imaging 2012;35:795-803
38. Christ A, Kainz W, Hahn EG, et al. The virtual family--development of surface-based anatomical models of two adults and two children for dosimetric simulations. Phys Med Biol 2010;55:N23-38
39. Tagliati M, Jankovic J, Pagan F, et al. Safety of MRI in patients with implanted deep brain stimulation devices. Neuroimage 2009;47 Suppl 2:T53-57
40. Rezai AR, Finelli D, Nyenhuis JA, et al. Neurostimulation systems for deep brain stimulation: in vitro evaluation of magnetic resonance imaging-related heating at 1.5 tesla. J Magn Reson Imaging 2002;15:241-250
41. Elwassif MM, Kong Q, Vazquez M, Bikson M. Bio-heat transfer model of deep brain stimulation-induced temperature changes. J Neural Eng 2006;3:306-315
42. Angelone LM, Ahveninen J, Belliveau JW, Bonmassar G. Analysis of the role of lead resistivity in specific absorption rate for deep brain stimulator leads at 3T MRI. IEEE Trans Med Imaging 2010;29:1029-1038
43. Shrivastava D, Abosch A, Hughes J, et al. Heating induced near deep brain stimulation lead electrodes during magnetic resonance imaging with a 3 T transceive volume head coil. Phys Med Biol 2012;57:5651-5665
44. Golestanirad L, Keil B, Angelone LM, Bonmassar G, Mareyam A, Wald LL. Feasibility of using linearly polarized rotating birdcage transmitters and close-fitting receive arrays in MRI to reduce SAR in the vicinity of deep brain simulation implants. Magn Reson Med 2017;77:1701-1712
45. Feng S, Qiang R, Kainz W, Chen J. A technique to evaluate MRI-induced electric fields at the ends of

practical implanted lead. IEEE Trans Microw Theory Tech 2015;63:305-313
46. Park SM, Kamondetdacha R, Nyenhuis JA. Calculation of MRI-induced heating of an implanted medical lead wire with an electric field transfer function. J Magn Reson Imaging 2007;26:1278-1285
47. American Society for Testing and Materials International, Designation: ASTM F2119-07, standard test method for evaluation of MR image artifacts from passive implants. West Conshohocken, PA: ASTM International, 2007
48. ASTM F2182-09 Standard test method for measurement of radio frequency induced heating on or near passive implants during magnetic resonance imaging. West Conshohocken, PA: ASTM, 2009
49. Neufeld E, Kuhn S, Szekely G, Kuster N. Measurement, simulation and uncertainty assessment of implant heating during MRI. Phys Med Biol 2009;54:4151-4169
50. Attaran Ali, Handler WB, Wawrzyn K, Chronik BA. Electric field probe for time-domain monitoring of radio frequency exposure during development and evaluation of MRI-conditional medical devices at 3 T. IEEE Trans Antennas Propag 2019;67:1854-1861
51. Mosallaei H, Sarabandi K. A one-layer ultra-thin meta-surface absorber. 2005 IEEE Antennas and Propagation Society International Symposium 2005:615-618
52. Lagovsky BA. Thin wide-band radio absorbing coatings. Proc 12th Int Conf Microw Telecommun Technol 2002:424-425
53. Sarto MS, Caneva C, De Rosa IM, Sarasini F, Sarto F, Tamburrano A. Design and realization of transparent absorbing shields for RF EM fields. Proc IEEE Antennas Propag Soc Int Symp 2006:668-671
54. Favazza CP, King DM, Edmonson HA, et al. Use of a radio frequency shield during 1.5 and 3.0 Tesla magnetic resonance imaging: experimental evaluation. Med Devices (Auckl) 2014;7:363-370
55. Yang R, Zheng J, Wang Y, Guo R, Kainz W, Chen J. An absorbing radio frequency shield to reduce RF heating induced by deep brain stimulator during 1.5-T MRI. IEEE T Electromagn C 2019;61:1726-1732
56. Teeuwisse WM, Brink WM, Haines KN, Webb AG. Simulations of high permittivity materials for 7 T neuroimaging and evaluation of a new barium titanate-based dielectric. Magn Reson Med 2012;67:912-918
57. Mattei E, Lucano E, Censi F, Angelone LM, Calcagnini G. High dielectric material in MRI: numerical assessment of the reduction of the induced local power on implanted cardiac lead. Conf Proc IEEE Eng Med Biol Soc 2016;2016:2361-2364
58. Brink WM, Webb AG. High permittivity pads reduce specific absorption rate, improve B1 homogeneity, and increase contrast-to-noise ratio for functional cardiac MRI at 3 T. Magn Reson Med 2014;71:1632-1640
59. Yu Z, Xin X, Collins CM. Potential for high-permittivity materials to reduce local SAR at a pacemaker lead tip during MRI of the head with a body transmit coil at 3 T. Magn Reson Med 2017;78:383-386
60. Ladd ME, Quick HH. Reduction of resonant RF heating in intravascular catheters using coaxial chokes. Magn Reson Med 2000;43:615-619
61. Yeung CJ, Karmarkar P, McVeigh ER. Minimizing RF heating of conducting wires in MRI. Magn Reson Med 2007;58:1028-1034
62. Bottomley PA, Kumar A, Edelstein WA, Allen JM, Karmarkar PV. Designing passive MRI-safe implantable conducting leads with electrodes. Med Phys 2010;37:3828-3843
63. Das R, Yoo H. Innovative design of implanted medical lead to reduce MRI-induced scattered electric fields. Electron Lett 2013;49:323-324
64. Das R, Yoo H. RF heating study of a new medical implant lead for 1.5 T, 3 T, and 7 T MRI systems. IEEE T Electromagn C 2017;59:360-366
65. Golestanirad L, Angelone LM, Kirsch J, et al. Reducing RF-induced heating near implanted leads through high-dielectric capacitive bleeding of current (CBLOC). IEEE Trans Microw Theory Tech 2019;67:1265-1273
66. Shrivastava D, Abosch A, Hanson T, et al. Effect of the extracranial deep brain stimulation lead on radiofrequency heating at 9.4 Tesla (400.2 MHz). J Magn Reson Imaging 2010;32:600-607
67. Golestanirad L, Angelone LM, Iacono MI, Katnani H, Wald LL, Bonmassar G. Local SAR near deep brain stimulation (DBS) electrodes at 64 and 127 MHz: A simulation study of the effect of extracranial loops. Magn Reson Med 2017;78:1558-1565
68. Abraham R, Ibrahim TS. Proposed radiofrequency phased-array excitation scheme for homogenous and localized 7-Tesla whole-body imaging based on full-wave numerical simulations. Magn Reson Med 2007;57:235-242
69. Eryaman Y, Akin B, Atalar E. Reduction of implant RF heating through modification of transmit coil electric field. Magn Reson Med 2011;65:1305-1313
70. Corcoles J, Zastrow E, Kuster N. Convex optimization of MRI exposure for mitigation of RF-heating from active medical implants. Phys Med Biol 2015;60:7293-7308
71. Xin SX, Huang Q, Gao Y, Li B, Xu Y, Chen W. Fetus MRI at 7 T: Shimming strategy and SAR safety implications. IEEE Trans Microw Theory Tech 2013;61:2146-2152
72. Van den Berg CA, van den Bergen B, Van de Kamer JB, et al. Simultaneous B1 + homogenization and specific absorption

rate hotspot suppression using a magnetic resonance phased array transmit coil. Magn Reson Med 2007;57:577-586
73. van den Bergen B, Van den Berg CA, Bartels LW, Lagendijk JJ. 7 T body MRI: B1 shimming with simultaneous SAR reduction. Phys Med Biol 2007;52:5429-5441
74. Gudino N, Sonmez M, Yao Z, et al. Parallel transmit excitation at 1.5 T based on the minimization of a driving function for device heating. Med Phys 2015;42:359-371
75. Yoo H, Gopinath A, Vaughan JT. A method to localize RF B(1) field in high-field magnetic resonance imaging systems. IEEE Trans Biomed Eng 2012;59:3365-3371
76. Carr JJ. Danger in performing MR imaging on women who have tattooed eyeliner or similar types of permanent cosmetic injections. AJR Am J Roentgenol 1995;165:1546-1547
77. Wagle WA, Smith M. Tattoo-induced skin burn during MR imaging. AJR Am J Roentgenol 2000;174:1795
78. Franiel T, Schmidt S, Klingebiel R. First-degree burns on MRI due to nonferrous tattoos. AJR Am J Roentgenol 2006;187:W556
79. Vahlensieck M. Tattoo-related cutaneous inflammation (burn grade I) in a mid-field MR scanner. Eur Radiol 2000;10:197
80. Ross JR, Matava MJ. Tattoo-induced skin "burn" during magnetic resonance imaging in a professional football player: a case report. Sports Health 2011;3:431-434
81. Dempsey MF, Condon B. Thermal injuries associated with MRI. Clin Radiol 2001;56:457-465
82. Alsing KK, Johannesen HH, Hvass Hansen R, Dirks M, Olsen O, Serup J. MR scanning, tattoo inks, and risk of thermal burn: an experimental study of iron oxide and organic pigments: effect on temperature and magnetic behavior referenced to chemical analysis. Skin Res Technol 2018;24:278-284
83. Nakamura T, Fukuda K, Hayakawa K, et al. Mechanism of burn injury during magnetic resonance imaging (MRI)--simple loops can induce heat injury. Front Med Biol Eng 2001;11:117-129
84. Lee SH, Barg JS, Yeo SJ, Lee SK. High-resolution numerical simulation of respiration-induced dynamic B0 shift in the head in high-field MRI. Investing Magn Reson Imaging. Investig Magn Reson Imaging 2019;23:38-45
85. Kim JM, Lee C, Hong SD, Kim JH, Sun K, Oh CH. T1-based MR temperature monitoring with RF field change correction at 7.0T. Investig Magn Reson Imaging 2018;22:218-228